ARMY RESEARCH LABORATORY

Multifunctional Structural-energy Storage Nanocomposites for Ultra Lightweight Micro Autonomous Vehicles (Final Report)

by Mark L. Bundy, Daniel P. Cole, Monica Rivera, and Shashi Karna

ARL-TR-6366 **February 2013**

NOTICES

Disclaimers

The findings in this report are not to be construed as an official Department of the Army position unless so designated by other authorized documents.

Citation of manufacturer's or trade names does not constitute an official endorsement or approval of the use thereof.

Destroy this report when it is no longer needed. Do not return it to the originator.

Army Research Laboratory
Aberdeen Proving Ground, MD 21005

ARL-TR-6366 **February 2013**

Multifunctional Structural-energy Storage Nanocomposites for Ultra Lightweight Micro Autonomous Vehicles (Final Report)

Mark L. Bundy, Daniel P. Cole, Monica Rivera, and Shashi Karna
Vehicle Technology Directorate, ARL

REPORT DOCUMENTATION PAGE

Form Approved
OMB No. 0704-0188

1. REPORT DATE *(DD-MM-YYYY)*	2. REPORT TYPE	3. DATES COVERED (From - To)
February 2013	DRI	October 2011 to September 2012

4. TITLE AND SUBTITLE
Multifunctional Structural-energy Storage Nanocomposites for Ultra Lightweight Micro Autonomous Vehicles (Final Report)

5a. CONTRACT NUMBER

5b. GRANT NUMBER

5c. PROGRAM ELEMENT NUMBER

6. AUTHOR(S)
Mark L. Bundy, Daniel P. Cole, Monica Rivera, and Shashi Karna

5d. PROJECT NUMBER
FY11-VTD-009

5e. TASK NUMBER

5f. WORK UNIT NUMBER

7. PERFORMING ORGANIZATION NAME(S) AND ADDRESS(ES)
U.S. Army Research Laboratory
ATTN: VTM
Aberdeen Proving Ground, MD 21005

8. PERFORMING ORGANIZATION REPORT NUMBER
ARL-TR-6366

9. SPONSORING/MONITORING AGENCY NAME(S) AND ADDRESS(ES)

10. SPONSOR/MONITOR'S ACRONYM(S)

11. SPONSOR/MONITOR'S REPORT NUMBER(S)

12. DISTRIBUTION/AVAILABILITY STATEMENT
Approved for public release; distribution unlimited.

13. SUPPLEMENTARY NOTES

14. ABSTRACT
A key concern in the design of micro autonomous vehicles is an onboard energy supply that is able to satisfy system power requirements while also limiting the mass/volume burden to the platform. The conventional solution is to increase the energy density of the power supply, typically a commercial battery. Another approach is to replace single-function structural components with multifunctional structural energy storage materials to supplement the main power supply. Here we report on the use of flexible carbon nanotube (CNT)-based composites for multifunctional structural energy storage applications. Supercapacitors were fabricated from aligned and non-aligned CNT-based polymer composites and were subject to electrical and mechanical characterization. In addition, an electromechanical characterization technique was used to explore the multifunctional behavior of the solid-state flexible supercapacitors. Initial tests showed that the specific capacitance of the composite materials increased by approximately 10% as the structure was subject to a 2% mechanical strain. These preliminary results indicate that these multifunctional solid-state composites could potentially replace micro vehicle flexible structural components, supplement system power requirements, and ultimately increase platform endurance.

15. SUBJECT TERMS
Micro vehicle, Supercapacitor, Carbon Nanotubes, CNTs, Energy Storage, Multifunctional Materials

16. SECURITY CLASSIFICATION OF:			17. LIMITATION OF ABSTRACT	18. NUMBER OF PAGES	19a. NAME OF RESPONSIBLE PERSON
a. REPORT	b. ABSTRACT	c. THIS PAGE			Mark L. Bundy
Unclassified	Unclassified	Unclassified	UU	36	19b. TELEPHONE NUMBER (*Include area code*) (410) 278-4318

Contents

List of Figures

List of Tables

Acknowledgments

We would like to thank Matthew H. Ervin of the Sensors and Electronic Devices Directorate, James Snyder of the Weapons and Materials Research Directorate, and Geoff Slipher of the Vehicle Technology Directorate for helpful conversations on supercapacitor-related research.

INTENTIONALLY LEFT BLANK.

1. Objective

1.1 Introduction

A reoccurring issue for lightweight (mass ≤100 g), palm-sized, micro-vehicle (MV) platforms, and in particular micro aerial vehicle (MAV) platforms, is the lack of sufficient onboard power. Stringent size and weight constraints and demanding voltage and power requirements significantly limit the number and type of energy storage devices that can be housed in MVs. While most commercial and developmental MVs currently use commercial-off-the-shelf lithium polymer batteries for their energy storage needs, the capacity of these batteries can limit mission durations to the order of minutes and the weight of these batteries can account for up to 60% of the overall system mass (*1*).

One method to increase the vehicle endurance without adding mass to the system or sacrificing payload capabilities is to incorporate multiple functions into a single material or structure. For example, the body or chassis of a MV could be replaced with a multifunctional material that would serve as both the vehicle structure and a supplemental energy storage material. Multifunctional structural-energy storage materials could potentially improve vehicle performance by simultaneously performing multiple tasks, while decreasing the overall system volume and/or weight.

1.2 Related Work

This study sought to combine the following emerging research areas: (1) lightweight energy storage using carbon nanomaterials with specific surface areas on the order of 10^3 m^2/g (*2–7*) with (2) multifunctional structural energy storage materials (*8–12*). Carbon nanomaterials are particularly suitable building blocks for this type of application due to their inherent multifunctionality (excellent electrical, mechanical, and thermal properties) (*13*).

The initial focus of this research effort was on supercapacitor-based structures because of the electrode symmetry and relative ease of fabrication. Supercapacitors store electric energy in the double layer that exists at the electrode/electrolyte interface (*14*). Figure 1 is a schematic of a basic supercapacitor, which consists of a current collector, a porous electrode layer (carbon nanotubes [CNTs], in this case) infiltrated with an electrolyte (i.e., a liquid electrolyte, polymer gel electrolyte, or solid polymer electrolyte), a separator layer, a counter electrode-electrolyte layer, and a counter current collector (*15*). For mechanically robust supercapacitors, a polymer binder may also be required to support the electrode structure.

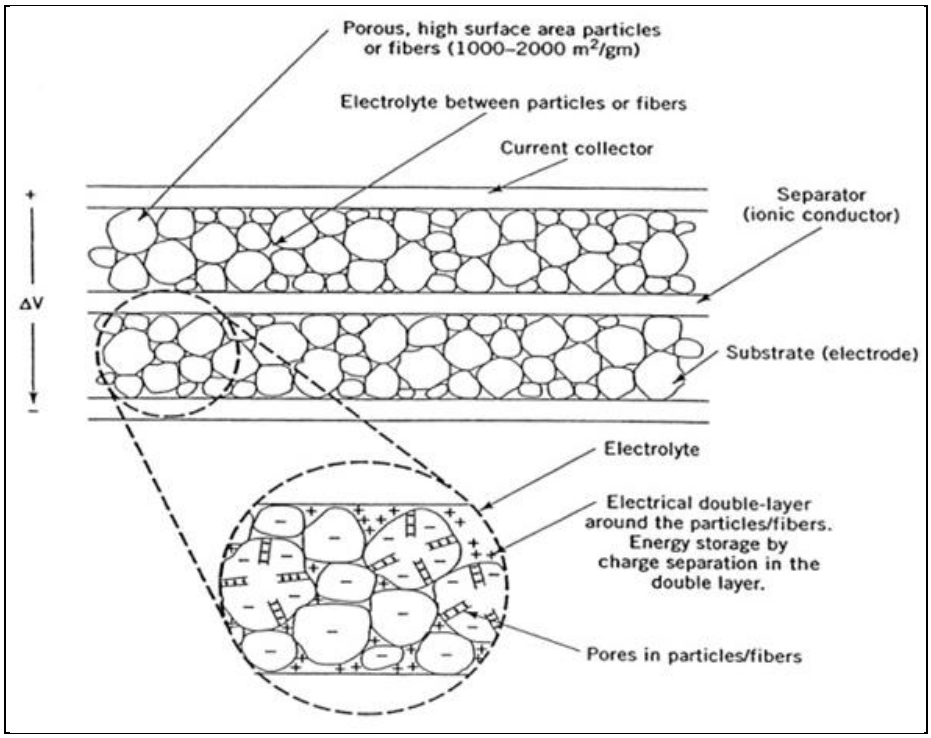

Figure 1. Schematic of a basic supercapacitor and subcomponents (*15*).

The focus of this effort was broken down into the following subtasks:

1. Process ultra-light, structurally robust, nanocomposite energy storage materials using aligned and non-aligned carbon nanomaterials as electrode building blocks; highly flexible cellulose and/or polymer substrates/binders; aqueous, organic, and solid polymer electrolytes; and flexible current collectors.
2. Characterize the electrical, mechanical, and electromechanical properties of the nanocomposite materials and supercapacitor subsystem components.
3. Characterize the effects of temperature and humidity on material performance.

2. Approach

2.1 Processing of Randomly Oriented CNT Electrodes

Randomly oriented electrodes (ROEs) were processed following a similar procedure reported by Hu et al. (*2*). Single wall carbon nanotubes (SWNTs) were used as the active material for the ROE electrodes. The SWNTs had an outer diameter of 1–2 nm and a length of 3–30 μm, as reported by the manufacturer (Cheap Tubes, Inc.). SWNTs (1–5 mg/mL) and a surfactant, sodium dodecylbenzenesulfonic acid (SDBS) (1–10 mg/mL), were dispersed in de-ionized water (DI-H_2O). The solution was stirred at approximately 600 rpm for 1 h, followed by probe

sonication (Sonics VibraCell) for 30 min at 100 W. The stirring/sonication steps were repeated and the resulting solution was coated on commercial copy paper (Quill Brand) using a size 45 Formed Meyer Rod (equivalent wire size of 0.045 in or 1.14 mm) (R.D. Specialties). The CNT-coated paper was allowed to dry for several days in a fume hood. Paper substrates were also coated with (1) pure DI-H_2O and (2) DI-H_2O + SDBS in order to calculate SWNT loading and establish baseline mechanical properties. Figure 2a shows an image of a SWNT electrode on a commercial paper substrate.

ROEs consisting of multi-walled nanotubes (MWNTs) (Cheap Tubes, Inc., outer diameter <8 nm) (80 wt.%) were also fabricated in this study. The MWNTs were dispersed in dimethylformamide (DMF), mixed with a polymer binder, polyvinylidene fluoride (PVDF) (Kynar Flex 2801), and deposited onto one side of a stainless steel current collector. Figure 2b shows an image of a MWNT electrode.

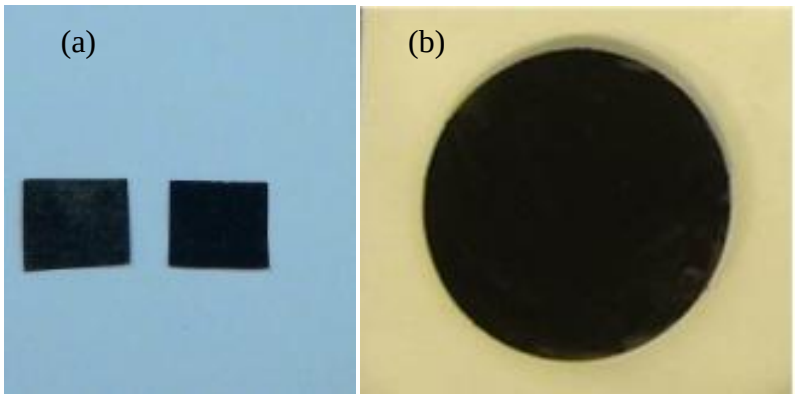

Figure 2. Randomly oriented CNT electrodes on (a) commercial paper substrates and (b) a stainless steel disc. Electrodes are approximately 1 cm wide in each image.

2.2 Processing of Vertically Aligned CNT Electrodes

Vertically aligned CNT forests were grown via a water-assisted chemical vapor deposition (CVD) method at Rice University (*16*). A catalyst layer consisting of aluminum (~10 nm) and iron (~1.5 nm) was first sputter deposited onto silicon (Si) wafers. For the CVD process, the carbon source used was ethylene gas, while an argon/hydrogen mixture run through a water bubbler was used as the carrier gas. The aligned CNTs were grown in a tube furnace held at 775 °C.

The aligned CNT polymer composite electrodes were prepared by infiltrating the CNT forests with a liquid polymer solution. One of the solutions tested in this work comprised of polydimethylsiloxane (PDMS) (Sylgard 184, Dow Corning®) and PVDF. PDMS was used to increase the flexibility of the composite, while the PVDF was chosen to bind the active electrode material together. In this study, several combinations of polymer compositions were investigated. The PDMS-PVDF polymer solutions were prepared via a combination of stirring and sonication followed by a period (~30 min) of degassing under low vacuum. The degassed

polymer solution was then poured onto the vertically aligned CNT forest and allowed to cure in an ambient environment. The vertically aligned electrodes (VAEs) were then cut to size and weighed.

Neat polymer matrices were also fabricated for baseline mechanical testing. Four different polymer compositions were investigated: 100:0, 90:10, 80:20, and 70:30 wt.% PDMS:PVDF.

We note that several combinations of polymers/solvents were attempted for the forest infiltration process; however, the solutions containing solvents tended to cause the forests to collapse. The collapsing effect was thought to be a result of relatively high capillary forces acting on the loosely rooted CNTs in the presence of a solvent. The selection of the solvent-free PDMS/PVDF solution allowed the CNT architecture to remain largely intact (figure 3a). This effect was at least partially due to air bubbles that formed in the liquid polymer during the magnetic stirring and probe sonication steps. The vacuum treatment step prior to infiltration was effective in removing the air bubbles and helped preserve the alignment of the CNT forest. The ability to preserve the CNT alignment during polymer infiltration was a key step in the processing of the electrodes, as even a partially collapsed CNT forest is expected to result in greatly reduced capacitance due to the large reduction in electrode surface area. After allowing the composite to cure in air overnight, the sample was lifted off from the substrate using a razor blade. Figure 3b displays the flexibility of the aligned CNT-PDMS/PVDF composite electrode.

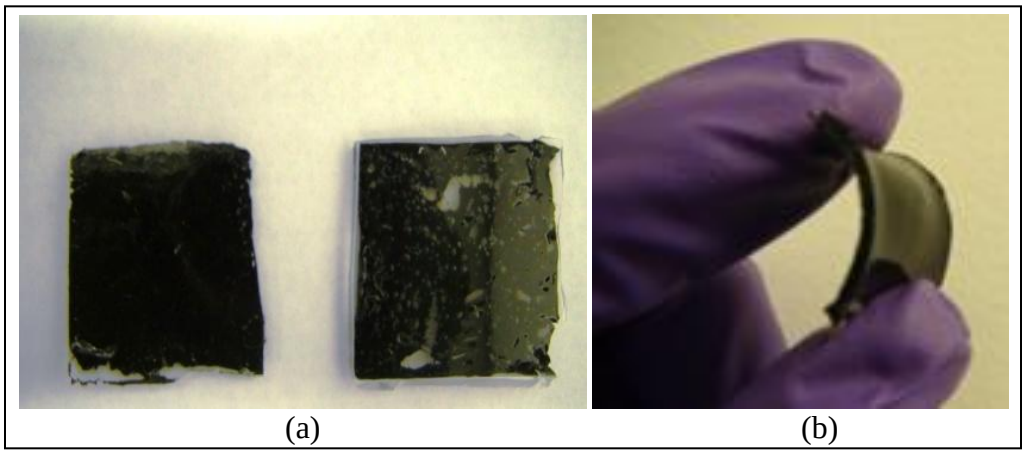

Figure 3. (a) Aligned CNT electrode with (left) and without (right) liquid polymer vacuum treatment. Note partially collapsed forest in electrode processed without the vacuum treatment step. (b) Image shows the inherent flexibility of aligned CNT electrode.

2.3 Nafion® Based Electrodes

Solid polymer electrolyte-aligned CNT composite electrodes were processed by infiltrating the aligned forests with Nafion 115 solution (5 wt.% in aliphatic alcohols, Sigma Aldrich). Nafion is a polymer electrolyte that has been used extensively for fuel cell applications (*17*). The polymer contains sulfonic acid groups and is ionically conductive without blending in other electrolytes (*18*). The aligned forests on Si substrates were heated to 60 °C using a hot plate. The Nafion

solution was pipetted onto the top of the CNTs and allowed to infiltrate the forest. The solvent was allowed to evaporate, and the process was repeated until the polymer electrolyte filled the forests and covered the tips of the CNTs. It should be noted that this uniform polymer layer covering the top of the CNT forests served as the separator later. The samples were removed from the hot plate and allowed to dry in air for 24 h. The composite films were then peeled from the substrates, resulting in free standing and flexible electrodes.

2.4 Micro-vehicle Structural Materials

As we are developing our structural-supercapacitors for MV applications, we first wanted to examine the material properties of an existing flexible MV platform. The ultimate goal for this work would be to replace a section of single-function structural material on the platform with a flexible structural supercapacitor that could provide supplemental power during high usage situations (i.e., accelerations). For this aspect of the project, we choose to examine the chassis material of the Dynamic Autonomous Sprawled Hexapod (DASH) and DynaRoACH robotic platforms created by the Biomimetic Millisystems Laboratory at the University of California Berkeley (*19–21*). The DASH and DynaRoACH were examined because these palm-sized biomimetic devices are flexible and constructed from readily available materials. The chassis of the DASH and DynaRoACH consist of lightweight four-ply poster board, adhesive, and a thin layer of polyethylene terephthalate (PET), sandwiched between a flexible interconnecting robotic section (e.g., body to leg joint). The components are laser cut into predetermined shapes and sandwiched together via heated rollers. The PET undergoes a high degree of bending in the devices and the mechanical properties of polymer are readily available (elastic modulus = 1.8–5.2 GPa and an ultimate tensile strength of 22–155 MPa [*22*]); we focused our initial efforts on determining the mechanical properties of the poster board material used in these platforms.

2.4.1 Supercapacitor Assembly

Aqueous, organic, and solid polymer based electrolytes were examined in this study. For the aqueous based devices, 6 M potassium hydroxide (KOH)/deionized water solution was used. A 1 M lithium hexafluorophosphate ($LiPF_6$) in 1:1 volume/volume mixture of ethylene carbonate (EC) and dimethyl carbonate (DMC) was used for the organic electrolyte. Supercapacitors assembled with the organic electrolyte were assembled in an argon-filled glovebox. Dried (in 50% relative humidity environment) Nafion was used for the solid polymer electrolyte (SPE), described above. Supercapacitors fabricated purely for electrical characterization were assembled in a modified two electrode Swagelok cell (figure 4a). The Swagelok ultra-torr vacuum fitting is ideal for basic supercapacitor and battery research as it allows for easy device assembly and reduces electrolyte evaporation and contamination. The spring mechanism in the test cell applies a constant, even pressure to the current collectors throughout the test process, thereby ensuring that adequate contact is made between the supercapacitor sub-components (figure 4b). In order to ensure an electrical path through only the supercapacitor, the fitting is

electrically isolated from the supercapacitor components using a 3M transparency film (PP22500).

A variety of current collectors were explored in this work including (a) silver adhesive (Electron Microscopy Sciences Silver Adhesive 503), (b) sputtered gold films, and (c) silver conductive ink (DuPont, CB028). The conductive silver ink appears to be an excellent choice for multifunctional device applications due to its flexibility and good electrical conductivity under mechanical strain.

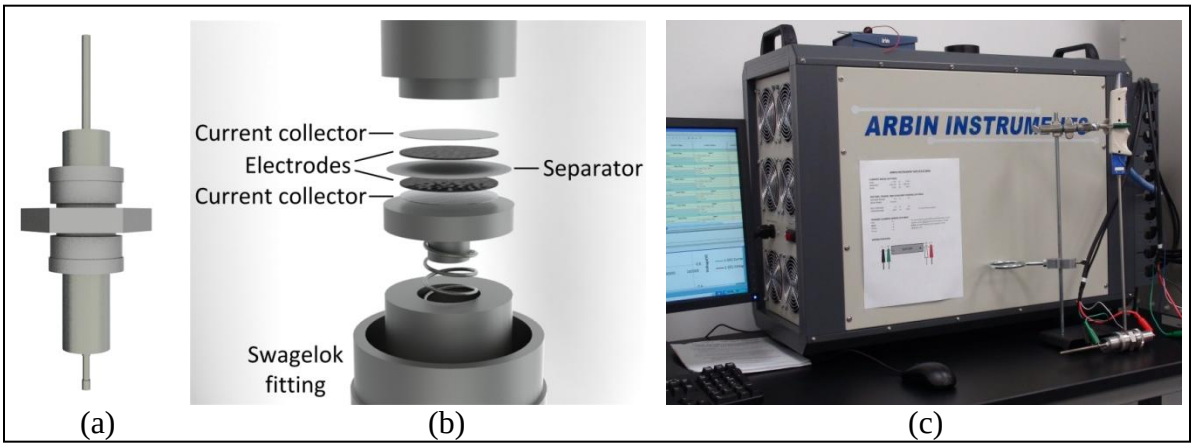

Figure 4. Electrical characterization equipment: (a) assembled Swagelok electrical test cell, (b) expanded view of the Swagelok electrical test cell with supercapacitor components, and (c) Arbin Instruments Supercapacitor Test System.

2.5 Electrical Characterization

Galvanostatic charge-discharge, self-discharge, and cyclic voltammetry (CV) test schedules were developed in the MITS Pro Testing Software (Arbin Instruments) and implemented on an Arbin Instruments Supercapacitor Testing System (see figure 4c). The measured capacitance (C_m), specific capacitance, energy density, and coulombic efficiency were approximated according to the methods outlined by Meng et al. (*5*).

$$C_m = \frac{I}{dU/dt} \tag{1}$$

where I is the applied current in the full cell and U is the potential difference. The specific capacitance of the device C_s can be defined as follows:

$$C_s = \frac{C_m}{M_e}, \tag{2}$$

where M_e is the total CNT mass contained within the two electrodes. Assuming that the mass and capacitance of the individual electrodes that make up the full supercapacitor are equivalent, C_m can also be used to determine the specific energy density, E_s, which is defined as follows:

$$E_s = \frac{C_m U^2}{2M_e}. \quad (3)$$

The coulombic efficiency, η, of the device is defined as

$$\eta = 100\% * \frac{Q_d}{Q_c} = 100\% * \frac{It_d}{It_c} = 100\% * \frac{t_d}{t_c}, \quad (4)$$

where Q_d is the charge associated with the discharge process, Q_c is the charge associated with the charging process, t_c is the time required to fully charge the supercapacitor, and t_d is the time required to fully discharge the supercapacitor.

The self-discharge characteristics of the ROE- and VAE-based supercapacitors were examined by measuring the leakage current or the current required to hold the supercapacitors at the charged potential (1.0 V for ROE-based supercapacitors and 2.5 V for VAE-based supercapacitors) for a given amount of time (0, 0.5, 1, and 10 h) and by measuring the voltage decay after the charging current is removed. The self-discharge behavior of a supercapacitor is a key indicator of device performance as the spontaneous loss of voltage causes the supercapacitor to approach a condition where power is required to reset the device to the charged functional state. For experiments where the charge hold time (t_h) was less than 10 h, the voltage decay measurements were stopped after a period of 2 h, and the final voltage was recorded (V_2). For prolonged discharge tests ($t_h \geq$ 10 h), the voltage was recorded for a minimum of 100 h after the charge current was removed. In an effort to compare the self-discharge behavior of the supercapacitors, and the half-life ($t_{1/2}$) and one-quarter life ($t_{1/4}$) of the supercapacitors were determined.

2.6 Mechanical Characterization

The mechanical properties of the materials used in this study were characterized via (1) an Instron 5965 Materials Testing System with a 500 N load cell and (2) a Deben Microtensile Stage with a 200 N load cell. For the Instron system, an environmental chamber with a custom humidity control system was used. Mechanical tests on the MV poster board material were conducted within the environmental chamber at a temperature of 72 ± 2 °F (22.2 ± 1.1 °C), and a relative humidity of 30 ± 3%. It should be noted that the elastic modulus calculated in these tests was estimated through the average strain, which was measured by the cross head movement. This method was applied in order to compare average mechanical properties of the materials to the corresponding average electrical properties of the materials (rather than mechanical properties at a single point via strain gage, etc.).

Mechanical tests were performed on supercapacitor filter papers in the dry and wet states. The properties of the wet filter paper are of interest because the separators used in some of the supercapacitors were soaked with liquid electrolyte. The wet condition was achieved by placing 50 µL of distilled deionized water on the samples. Although 6 M KOH and 1 M $LiPF_6$ in EC:DMC are used for the actual supercapacitor assembly, distilled deionized water was used for these initial tests instead of the actual electrolytes so as not to damage the mechanical grips.

2.6.1 Electrical Characterization with *In Situ* Microtensile Testing

The multifunctional behavior of individual supercapacitor components and full solid-state supercapacitor structures was characterized by studying the electrical properties during microtensile testing. These experiments were a major focus of this research effort as it quantified under what mechanical loading conditions the supercapacitor could perform. The Deben Microtest 200 N Tensile Stage was altered to allow electrical connections within the grips to contact the specimen current collectors (figure 5). The specimen and contacts were electrically isolated from the microtensile stage. Several tests with the altered microtensile stage configuration were compared to the normal stage setup to show that the electrical connections had no appreciable effect on the load cell readings.

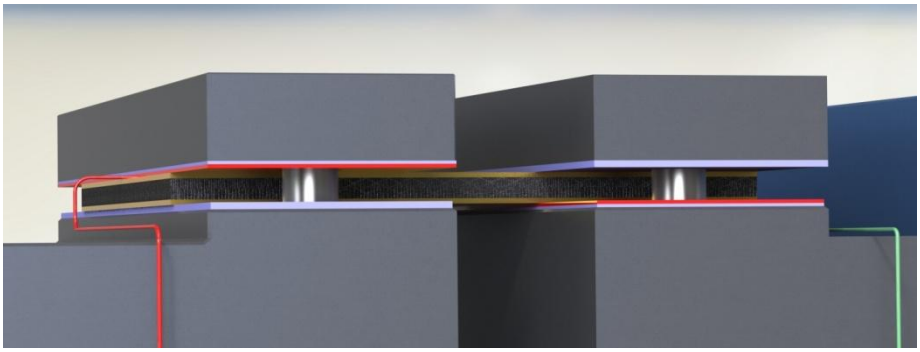

Figure 5. Schematic of microtensile stage altered for *in situ* electrical characterization. The conductive red films contact the specimen current collectors, while the non-conductive blue films isolate the sample/contacts from the grips.

3. Results

3.1 Microscopy

Figure 6 shows transmission electron microscopy (TEM) and scanning electron microscopy (SEM) images of the aligned CNT forests grown by collaborators at Rice University. The TEM images were used to show that the aligned forest consisted of CNTs with approximately 6–10 walls. Figure 7 shows SEM images of the CNT-coated papers. The large fibers seen in figure 7a are the paper cellulose fibers. Figure 7b appears to show the existence of 1–10 μm CNT agglomerates on the surface of the paper. Figures 7c and d appear to show dispersed CNTs on the paper substrate in between the agglomerates. The presence of agglomerates would indicate that the mechanical mixing and sonication steps were not entirely successful in dispersing the CNTs. The agglomerates are expected to lead to a lower specific capacitance than is theoretically possible due to the large percentage of active material inaccessible to the electrolyte.

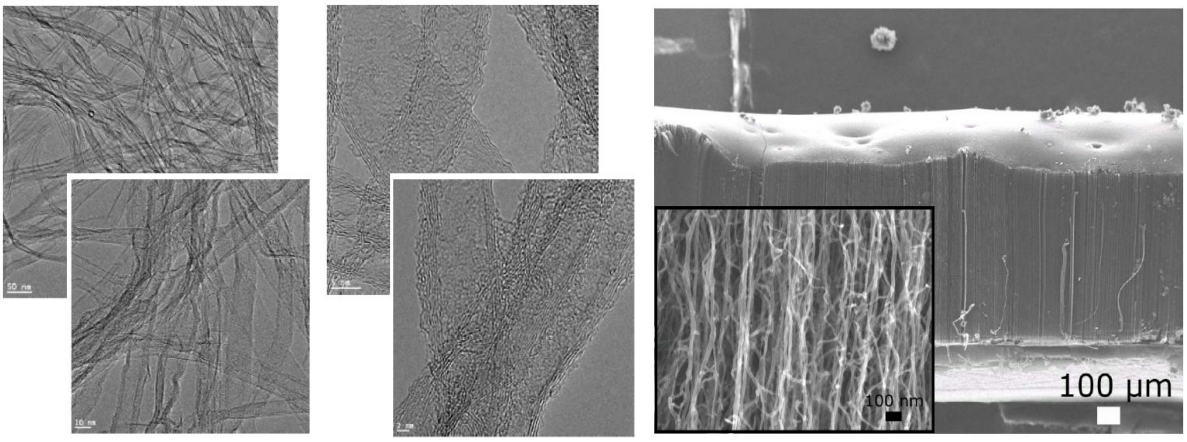

Figure 6. TEM (left) and SEM (right) images of aligned CNT forests grown by collaborators at Rice University (*16*).

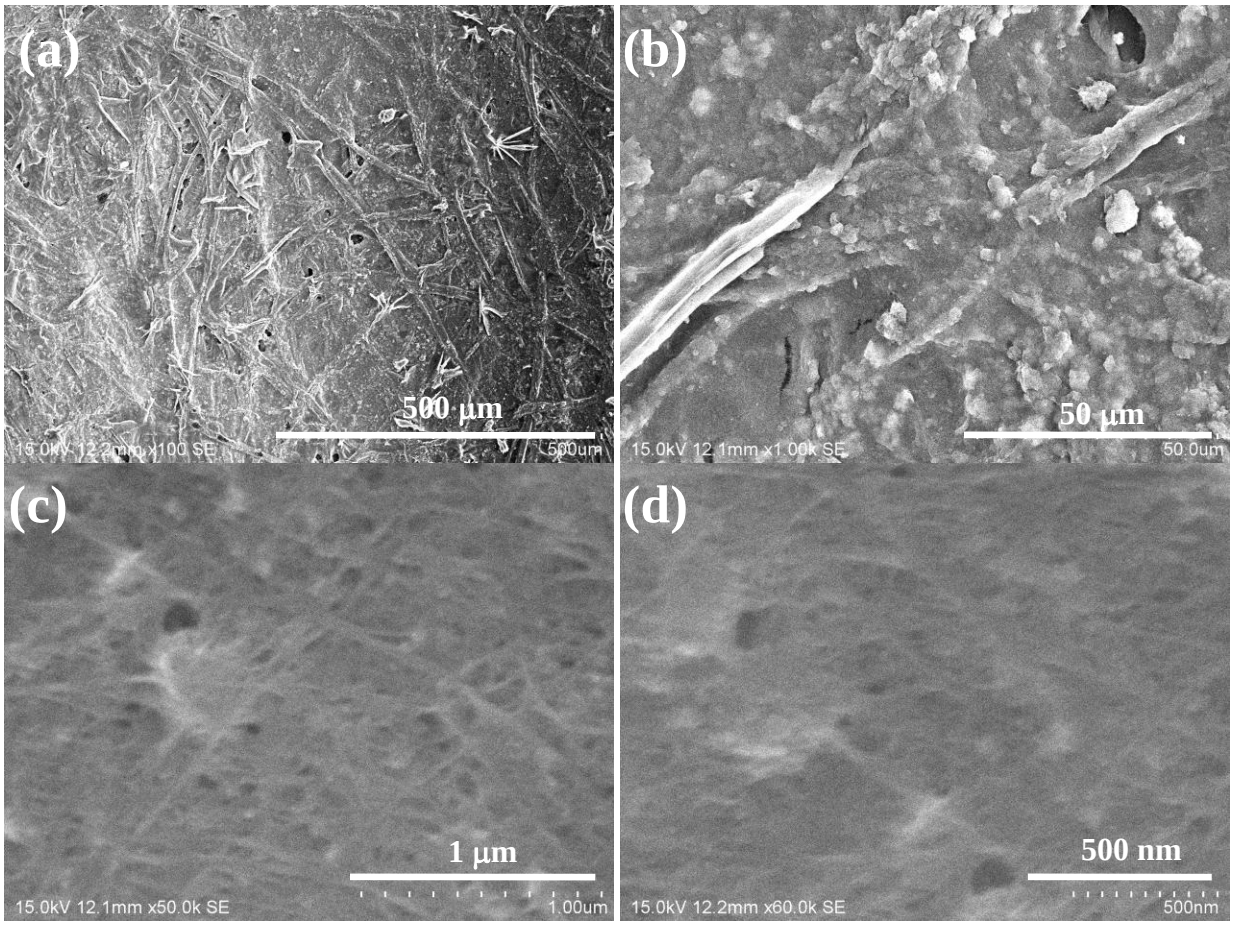

Figure 7. SEM images of commercial paper coated with CNT-based ink. (a) Cellulose fibers of substrate material, (b) 1–10 µm CNT agglomerates indicate that mixing/sonication steps were not entirely successful, and (c) and (d) dispersed CNTs on substrate in between agglomerates.

Figure 8 shows an SEM image of the cross section of an aligned CNT forest infiltrated with Nafion. The alignment of the CNT network appears to be preserved, which would indicate that that the high specific surface area of the CNTs is available for a high degree of electrolyte-electrode interaction.

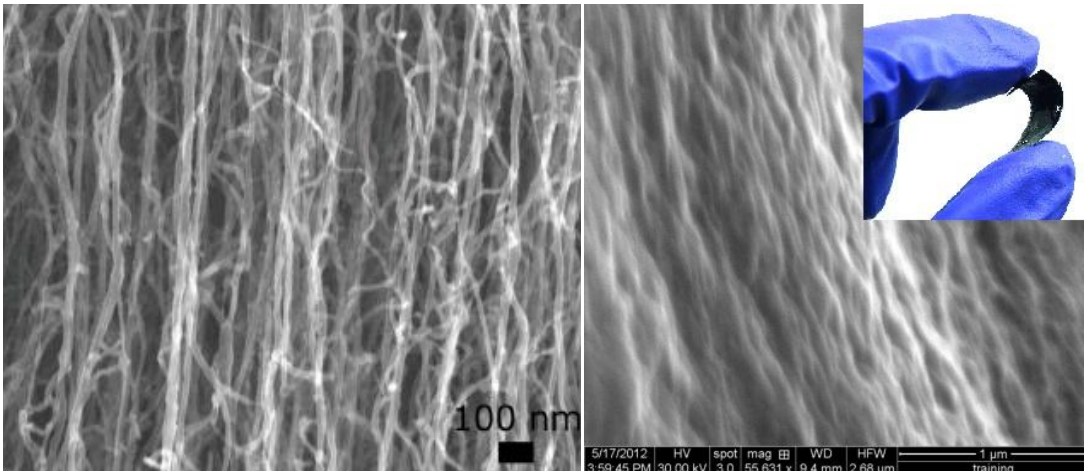

Figure 8. SEM image of an aligned CNT forest (left) before and (right) after Nafion infiltration. Note that alignment of forest appears to be preserved post infiltration. Inset of right figure shows flexibility of solid-state CNT-solid polymer electrolyte composite.

3.1.1 Mechanical Characterization Results

3.1.1.1 CNT-coated Paper Electrodes

Table 1 summarizes the mass loading and micromechanical behavior of the SWNT-coated paper substrates. The mass of the (1) uncoated paper, (2) DI-water coated paper, (3) DI-water/SDBS coated paper, and (4) SWNT-coated paper were used to calculate an approximate active material (SWNT) mass loading of 500 $\mu g/cm^2$. These results also indicate that water is retained in the paper substrate after the coating process, even after several days of drying under the fume hood. This may partially explain the difference in mechanical properties for the uncoated and SWNT coated specimens. The elastic modulus of the paper substrate decreases by 15%–20% after the SWNT coating process; however, this result is similar to the paper substrates coated with pure water, suggesting the decrease in mechanical properties may be the result of increased water content in the paper (*23*).

Table 1. Mechanical properties and mass loading of CNT-coated copy paper.

Specimen	Specimen Mass (mg/cm^2)	Elastic Modulus (GPa)
Uncoated paper	7.6 ± 0.1	7.59 ± 0.44
Water coated paper	8.0 ± 0.2	6.17 ± 0.11
SDBS/water coated paper	8.2 ± 0.2	5.43 ± 0.28
SWNT coated paper	8.7 ± 0.2	6.34 ± 0.12

3.1.1.2 Mechanical Properties of Cellulose Filter Paper Separators and Substrates in Dry and Wet State

The manufacturer-supplied particle retention values (size at which a retention level of 98% of the total number of particle initially challenging filter is obtained [*24*]) and experimentally determined mechanical properties of cellulose filter paper properties can be found in table 2. Samples in the "dry" and "wet" state were tested in a controlled environment (30% relative humidity, 22 °C using custom-built humidity/temperature chamber). To ascertain general trends between the dry and wet samples, the values for the wet samples are represented as percentages of the dry mechanical values. There was significant variability for all filter paper grades tested, which is believed to partially be due to the variability in the machine direction (MD)/cross-machine direction (CD) angle with respect to the loading direction. The elastic modulus *E* and the tensile strength σ_t were significantly reduced while in the wet state, only retaining 3%–9% of their original values. Even in the dry state, the elastic modulus and tensile strength of all the cellulose filter papers tested in this study were significantly less than that of the poster board (will be shown in the MV platform materials section to be $E = 2.5 \pm 0.2\ GPa$ and $\sigma_t = 40 \pm 10\ MPa$). However, the ROE electrodes on the commercial paper have elastic properties more closely matched to the poster board properties (table 1). Another solution may be to print the CNT electrodes directly on the poster board material itself, although this would essentially add mass to the vehicle platform and may be a net system loss.

Table 2. Cellulose filter paper properties.

Grade	Particle Retention Liquid (µm)	E_d (MPa)	E_w (% of E_d) (MPa)	σ_{td} (MPa)	σ_{tw} (% of σ_{td}) (MPa)
G1	11	585–1163	8 ± 3%	8.4 – 11.7	3.8 ± 0.8 %
G2	8	773–1406	9 ± 4%	10.4 – 14.9	3.4 ± 0.4%
G3	6	454–906	3 ± 1%	6.8 – 9.6	4.2 ± 0.5%
G5	2.5	537–1213	7 ± 1%	7.8 – 9.5	8.9 ± 0.7%

Note: Particle Retention (Liquid) = particle size at which a retention level of 98% of the total number of particles initially challenging the filter is obtained [*24*]. Subscripts d and w signify "dry" and "wet" state.

3.2 Polymer Composite Matrices and Electrodes

The mechanical properties of the neat polymer composites binders are in table 3. As expected, E and σ_t increased with increasing PVDF composition; this was not surprising given the decreasing volume fraction of the relatively compliant PDMS. The pure PDMS sample was the outlier as it actually showed the highest measured tensile strength and an elastic modulus roughly equal to the modulus of the 90:10 composite. This could potentially be due to the poor mixing of the composite polymer samples, although microscopy has not yet been performed to verify this.

Table 3. Mechanical properties of neat polymer composites.

ID	Composition (PDMS:PVDF)	E (MPa)	σ_t (MPa)
1	100:0	1.07 ± 0.07	1.2 ± 0.3
2	90:10	0.9 ± 0.07	0.48 ± 0.05
3	80:20	1.7 ± 0.2	0.84 ± 0.05
4	70:30	2.6 ± 0.4	1.1 ± 0.3

Uniaxial tensile tests were also performed on the polymer infiltrated VAEs. Figure 9 compares the mechanical behavior of a neat PDMS (85 wt.%)–PVDF (15 wt.%) matrix and the same matrix loaded with approximately 8 wt.% vertically aligned CNTs. The average elastic modulus of the VAE and the neat polymer composite matrix was approximately 2.5 and 1.0 MPa, respectively. While the 250% increase in elastic modulus is notable, the configuration of the composite electrode is not currently designed to maximize the mechanical properties. Here, the CNTs in the electrode are aligned transverse to the direction of loading. As a result, the configuration does not take full advantage of the CNTs, which is typically realized through aligning the filler with the direction of mechanical loading (*25*, *26*). As with the cellulose filter papers, the elastic modulus on the order of 1 MPa for the PDMS/PVDF/CNT based electrodes is too compliant to replace the PET film ($1.8 - 5.2\ GPa$) used between poster board layers to link the vehicle body parts. However, the addition of the CNTs could allow for the ability to tune the mechanical properties to some degree for more compliant MV structures (*19–21*).

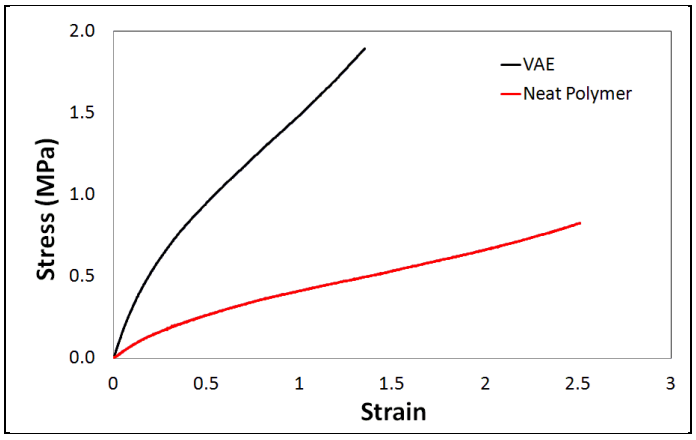

Figure 9. Tensile tests of polymer infiltrated VAE (8 wt.% CNTs) and a neat polymer composite reference sample (85:15 PDMS:PVDF).

3.3 Results of Micro-vehicle Platform Materials

As anticipated, the mechanical properties of the poster board were significantly different in the machine direction and cross-machine direction. In the machine direction $E = 2.5 \pm 0.2\ GPa$ and $\sigma_t = 40 \pm 10\ MPa$ while in the cross-machine direction $E = 0.78 \pm 0.04\ GPa$ and $\sigma_t = 13.6 \pm 0.8\ MPa$. The elastic modulus of the poster board in the machine direction was comparable to that of the PET film ($1.8 - 5.2\ GPa$) mentioned in the previous section. However, additional tests on the poster board in the supercapacitor configuration (under wet/dry conditions, coated with CNTs, current collectors, etc.) are required to verify if this is a suitable replacement for the single function structural materials used in these MV platforms.

3.3.1 Electrical Characterization Results

Figures 10 and 11 display the galvanostatic charge/discharge results for a CNT-coated paper based supercapacitor and a vertically aligned CNT-polymer based supercapacitor, respectively. The CNT-coated paper supercapacitor used a 6 M KOH aqueous electrolyte. The VAE-based supercapacitor consisted of a forest infiltrated with the 85:15 PDMS:PVDF blend and LiPF6 organic electrolyte. Various current collectors were explored for these supercapacitors including silver conductive ink, sputtered gold films, and silver paste.

Equation 1 was used to calculate the specific capacitance of the device, which ranged from approximately 1–10 F/g for both types of supercapacitors. It should be noted that the M_e used for these calculations was the carbon material present in both electrodes. These results are at least a full order of magnitude lower than liquid electrolyte based supercapacitors reported in the literature (*2–5*). The relatively low specific capacitance for the ROEs could be the result of CNT agglomerates seen in figure 7. The relatively low specific capacitance for the VAEs could be due to the lower ionic conductivity of the gel electrolyte (vs. liquid electrolytes) and/or the lower usable electrode surface area as the result of the forest collapsing effect discussed in section 2.

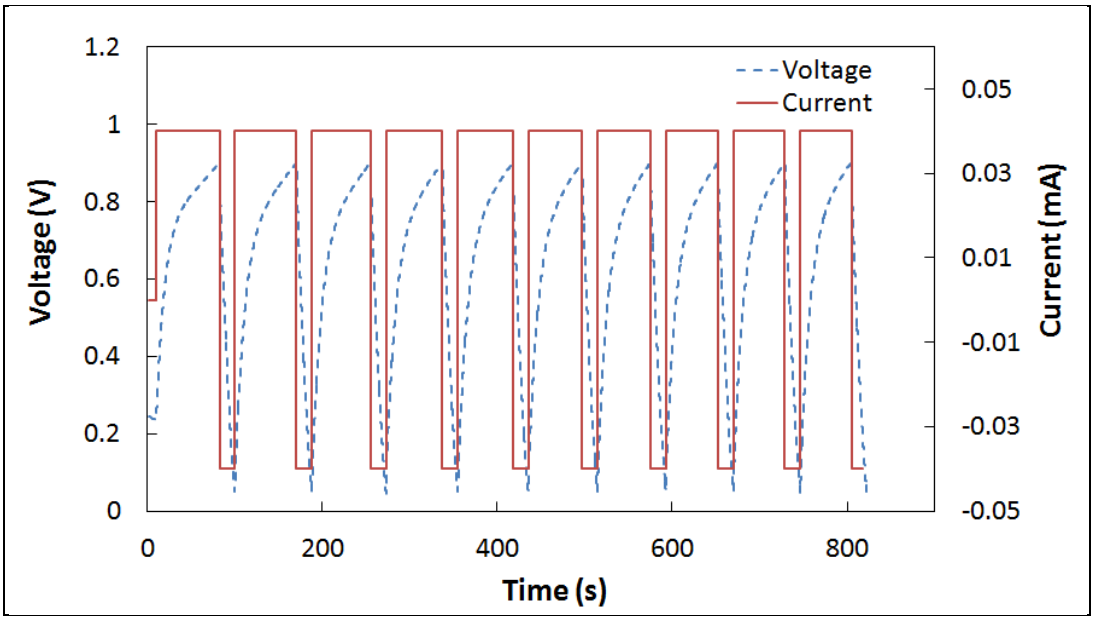

Figure 10. Galvanostatic charge/discharge results for supercapacitor consisting of ROE on commercial paper substrate, soaked with a 6 M KOH aqueous electrolyte and sputtered gold current collector. Current = ±0.04 mA.

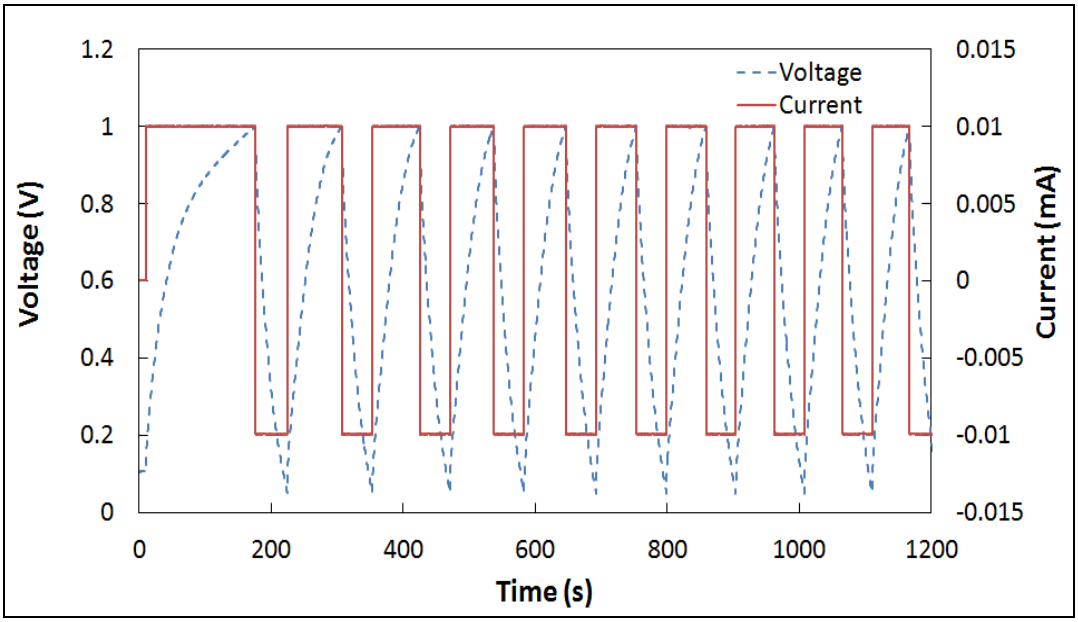

Figure 11. Galvanostatic charge/discharge results for VAE-based EDLC with 6 M $LiPF_6$ organic electrolyte with silver adhesive current collector. Current = ±0.01 mA.

3.3.2 Self-discharge of ROE and VAE-based Supercapacitors

Table 4 contains the self-discharge behavior for several ROE- and VAE-based supercapacitors. As the table indicates, the self-discharge behavior is dependent not only on the electrode composition but also on the initial charge current, I_c, and the t_h. From a self-discharge

standpoint, the VAE-based supercapacitors dramatically outperformed their ROE-based counterparts, with all devices retaining charge after a period of 2 h, regardless of charge hold time. This charge retention behavior is believed to be due to the binding of the electrolyte within the larger polymer matrix of the VAE-based supercapacitors (*5*).

Table 4. Supercapacitor self-discharge statistics. For $\boldsymbol{t_h}$ = 0, 0.5, and 1 h, information for cycle 5 is listed. For $\boldsymbol{t_h}$ = 10 h, information for cycle 1 is listed.

ROE-based Supercapacitors						**VAE-based Supercapacitors**					
ID	$\boldsymbol{I_c}$ **(mA)**	$\boldsymbol{t_h}$ **(h)**	$\boldsymbol{t_{1/4}}$ **(min)**	$\boldsymbol{t_{1/2}}$ **(min)**	$\boldsymbol{V_2}$ **(V)**	**ID**	$\boldsymbol{I_c}$ **(mA)**	$\boldsymbol{t_h}$ **(h)**	$\boldsymbol{t_{1/4}}$ **(min)**	$\boldsymbol{t_{1/2}}$ **(min)**	$\boldsymbol{V_2}$ **(V)**
ROE_{G1}	1	0	0.42	2.83	<0.05	$VAE_{90:10-Ag}$	0.05	0	0.02	0.39	0.26
	1	0.5	1.24	4.35	<0.05		0.05	0.5	0.57	14.70	0.66
	1	1	2.47	10.68	0.08		0.05	1	0.81	18.26	0.64
							0.1	0	0.02	0.26	0.05
							0.1	0.5	1.02	13.46	0.51
							0.1	1	1.05	19.32	0.70
ROE_{G2}	1	0	0.52	2.96	<0.05	$VAE_{80:20-Ag}$	0.05	0	0.52	13.68	0.58
	1	0.5	0.84	2.82	<0.05		0.05	0.5	2.08	25.02	0.74
	1	1	1.39	4.34	<0.05		0.05	1	1.63	27.26	0.77
							0.1	0	0.03	0.37	0.28
							0.1	0.5	0.62	8.75	0.52
							0.1	1	0.78	11.44	0.57
ROE_{G3}	1	0	0.13	0.51	<0.05	$VAE_{70:30-Ag}$	0.05	0	0.12	3.73	0.59
	1	0.5	2.99	11.99	0.06		0.05	0.5	1.11	17.17	0.72
	1	1	0.76	2.7	<0.05		0.05	1	0.67	15.12	0.74
							0.1	0	0.03	0.61	0.49
							0.1	0.5	0.06	4.78	0.69
							0.1	1	0.05	7.37	0.78
							0.1	10	1.5	132	2.21
ROE_{G4}	1	0	0.14	0.49	<0.05	$VAE_{90:10-SS}$	0.05	0	0.03	0.96	0.48
	1	0.5	2.75	10.94	<0.05		0.05	0.5	5.81	110.71	1.23
	1	1	1.88	7.88	<0.05		0.05	1	24.62	>120	1.51
							0.1	0	0.01	0.08	0.88
							0.1	0.5	12.65	>120	1.37
							0.1	1	2.52	32.46	0.76
							0.1	10	65	414	1.73

Figure 12a contains the leakage current of supercapacitors $VAE_{90:10-SS}$ and $VAE_{70:30-Ag}$ during a charge hold time of 10 h. The leakage current for the $VAE_{90:10-SS}$ device dropped significantly in the beginning of the charge hold process, from 0.1 mA to ~5.4 µA after the first 15 min and then gradually stabilized to around 2.6 µA after a period of approximately 4 h. The current drop for the $VAE_{70:30-Ag}$ device was much less significant, from 0.1 mA to 92.9 µA after 15 min, and continued to decay to a value of ~52.6 µA after a period of 10 h. The self-discharge behavior of $VAE_{90:10-SS}$ and $VAE_{70:30-Ag}$ after the 10-h charge hold process can be found in figure 12b. $VAE_{90:10-SS}$ lost 79.11% of its charge during the first day, with an initial, instantaneous drop of 0.0638 V (or 2.5% of its charged potential). $VAE_{70:30-Ag}$, on the other hand, lost 72.97% of its charge during the first day, with an initial, instantaneous drop of 0.2881 V (or 12% of its charged potential). $VAE_{70:30-Ag}$ retained a higher output voltage over prolonged periods.

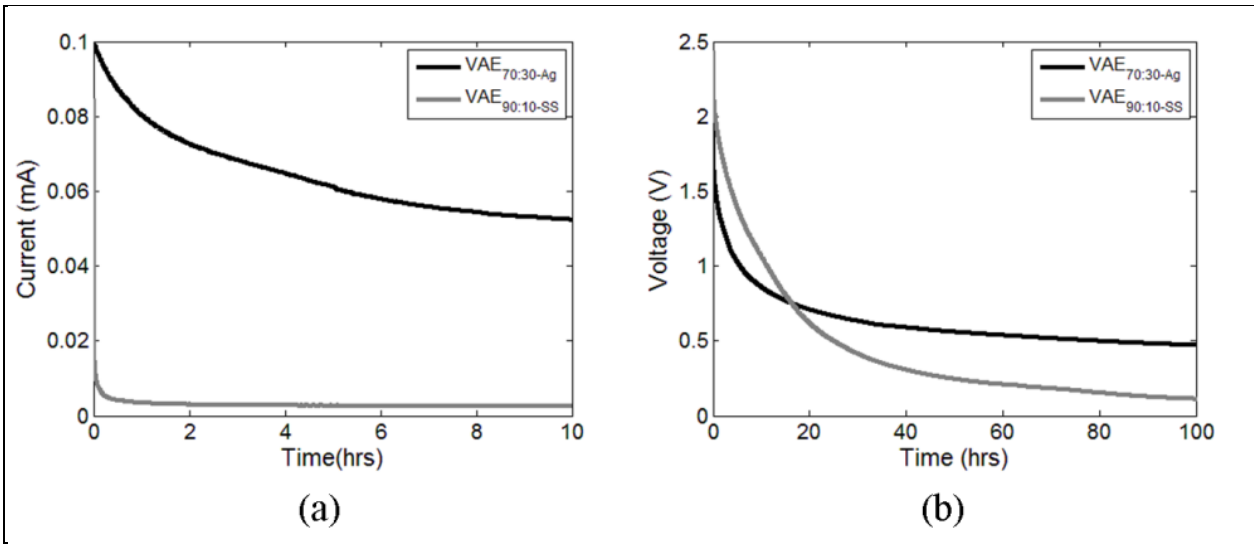

Figure 12. Supercapacitor leakage and self-discharge behavior. (a) Current applied to the supercapacitor to hold the voltage at 2.5 V. (b) Voltage decay after the charging current is removed.

3.4 Electromechanical Characterization Results

Figure 13 displays the results of the electrical characterization of a dry CNT ROE on a commercial paper substrate during *in situ* microtensile testing. The electrical resistance across the electrode surface was monitored as the sample was mechanically loaded. The electrical resistance was relatively constant throughout the elastic region and much of the plastic region of the ROE. The electrical resistance of the electrode appears to be relatively constant up to a mechanical strain of 2%. As the load begins to drop and the sample fractures, the electrical resistance quickly increases. The relatively high electrical resistance across the electrode is most likely due to the CNT agglomerates seen in figure 7. The use of a surfactant could also be causing the high electrical resistance (*4*). Increased mixing and sonication times are expected to provide increased CNT dispersion and more uniform coatings (*2*).

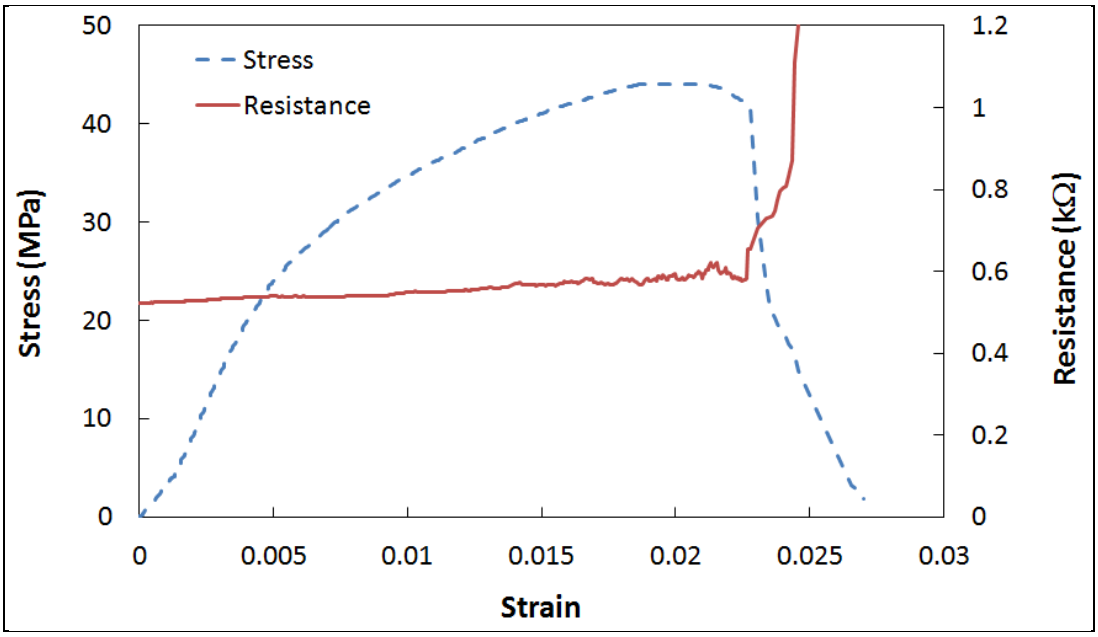

Figure 13. Electromechanical behavior of a CNT ROE on a commercial paper substrate.

Initial electromechanical tests were also performed on a working solid-state supercapacitor. An aligned CNT forest filled with a solid polymer electrolyte (Nafion, 50% relative humidity) and a flexible silver conductor ink current collector was subject to galvanostatic charge-discharge tests while under uniaxial mechanical load, as seen in the schematic in figure 14. The composite sample (~1 wt.% CNTs) was loaded and held at various stress conditions for charge/discharge cycles. The elastic modulus of the structure was approximately 100 MPa, which was similar to neat Nafion films tested in this study and also to Nafion membranes tested previously under similar environmental conditions (*27*). The lack of an increase in mechanical properties for the composite structure could indicate that the load is not effectively being transferred from the matrix to filler. Recall that the PVDF/PDMS composite electrode showed a 250% increase in the elastic modulus compared to the neat matrix, albeit with a CNT loading of approximately 8 wt%. As with the PVDF/PDMS composite, the direction of CNT alignment is transverse to the loading direction, which could also partially explain the lack of an increase in the mechanical stiffness.

In the unloaded state, the solid-state supercapacitor displayed a specific capacitance of approximately 5 F/g, when considering the active material mass in both electrodes. The specific capacitance actually increased by approximately 10% as the multifunctional structure was loaded to a 2% strain. Further loading of the structure caused the specific capacitance to drop, approximately to the value at the unloaded state, before mechanically failing at a strain of around 6%. Further tests are required to understand this behavior, but the effect may be similar to previously reported work on flexible, CNT-liquid electrolyte supercapacitors subject to various bending conditions (*2*, *4*). These initial tests suggest that the CNT-solid polymer electrolyte composite structures could potentially replace single function MV structural components with an

elastic modulus on the order of 100 MPa. An increase in the mechanical stiffness could be realized through higher CNT loadings or a decrease in the solid polymer matrix humidity (*27*), but may lead to a lower electrical performance.

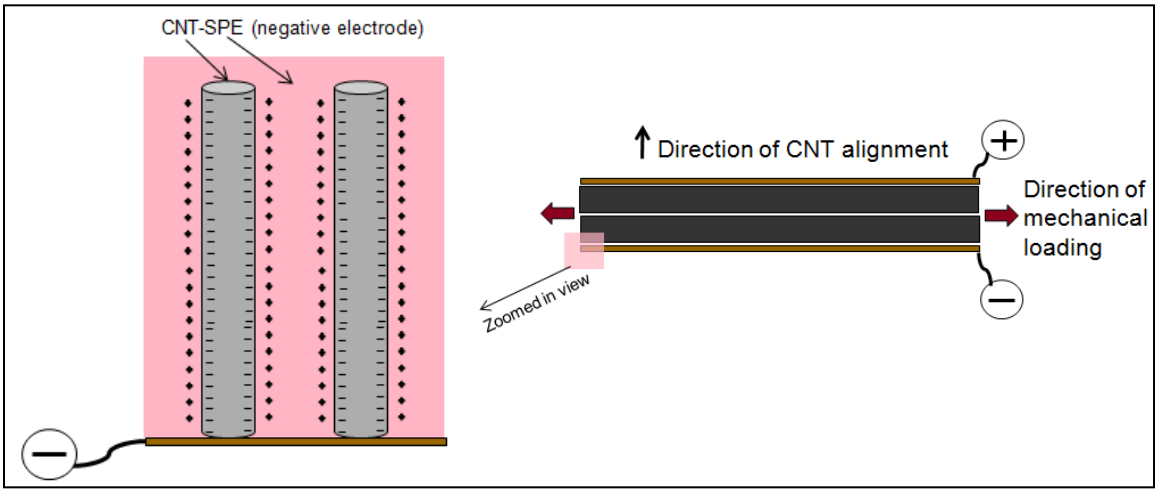

Figure 14. Schematic of CNT-Nafion supercapacitor under uniaxial mechanical load. Image on left is a zoomed in view of the double layer that exists at the negative electrode-electrolyte interface. Image on right is cross-sectional view of supercapacitor.

4. Conclusions

In summary, a variety of supercapacitors were developed for structural-energy storage applications. Supercapacitors were constructed from aligned and non-aligned CNT networks and were characterized through a variety of electrical, mechanical, and electromechanical techniques, which were the first and second objectives of this research effort. Uniaxial tensile tests were used to explore the mechanical properties of the supercapacitor subcomponent materials, while charge/discharge, CV, and self discharge tests were used to characterize the electrical properties of the materials. The mechanical properties of a flexible, structural poster board, similar to a material used previously in several flexible, biomimetic robots, were also examined. An electrical characterization technique with *in situ* microtensile testing was developed to explore the multifunctional behavior of the supercapacitor structures and supercapacitor subcomponent materials. Tests on an all solid-state CNT-Nafion supercapacitor showed that the specific capacitance increased by approximately 10% as the structure was elongated by 2%. These initial results indicate that the CNT-solid polymer electrolyte composites could potentially replace MV structural components of similar mechanical properties (elastic modulus ~100 MPa), while providing supplemental power to the platform with little to no weight penalty. The third and last objective of this project was to examine the environmental conditions on structure performance. These experiments are currently incomplete as of December 2012, although a custom humidity

chamber was recently designed and installed. Thus far, mechanical tests on the MV poster board material were examined at a single controlled humidity level, but additional tests are required to characterize the properties at various humidity conditions. In particular, the performance of the CNT-Nafion structures are expected to be closely linked to the environmental conditions as the ionic conductivity and mechanical properties of Nafion are partially controlled by the water content present in the material (*18, 27*).

5. References

1. Rivera, M. Current and Next-generation Energy Storage Devices for Micro Vehicle Applications. In *Proceedings of the SAE 2011 AeroTech Congress and Exhibition*, Toulouse, France, 2011.

2. Hu, L.; Choi, J.; Yang, Y.; Jeong, S.; Mantla, F.; Cui, L.; Cui, Y. Highly Conductive Paper for Energy-storage Devices. *PNAS* **2009**, *106*, 21490–21494.

3. Pushparaj, V.; Shaljumon, M.; Kumar, A.; Murugesan, S.; Ci, L.; Vajtai, R.; Linhardt, R.; Nalamasu, O.; Ajayan, P. Flexible Energy Storage Devices Based on Nanocomposite Paper. *PNAS* **2007**, *34*, 13574–13577.

4. Anton, C.; Ervin, M. *Carbon Nanotube Based Flexible Supercapacitors*; ARL-TR-5522; U.S. Army Research Laboratory: Adelphi, MD, 2011.

5. Meng, C.; Liu, C.; Chen, L.; Hu, C.; Fan, S. Highly Flexible and All-solid-state Paper Like Polymer Supercapacitors. *Nano Letters* **2010**, *10*, 4025–4031.

6. Ervin, M.; Raju, V. *Carbon Nanotube/Graphene Supercapacitors Containing Manganese Oxide Nanoparticles*; ARL-TR-6289; U.S. Army Research Laboratory: Adelphi, MD, 2012.

7. Ervin, M. H.; Mailly, B.; Palacios, T. Electrochemical Double Layer Capacitance of Metallic and Semiconducting SWCNTs and Single-Layer Graphene. *ECS Transactions* **2012**, *41* (22), 153–160.

8. Thomas, J.; Qidwai, M. The Design and Application of Multifunctional Structure-battery Materials Systems. *JOM* **2005**, *57*, 18–24.

9. Luo, X.; Chung, D. Carbon-fiber/Polymer-matrix Composites as Capacitors, *Composites Science and Technology* **2001**, *61*, 885–888.

10. Snyder, J.; Carter, R.; Wetzel, E. Electrochemical and Mechanical Behavior in Mechanically Robust Solid Polymer Electrolytes for Use in Multifunctional Structural Batteries. *Chemistry of Materials* **2007**, *19*, 3793–3801.

11. Gallagher, T.; Ciocanel, C.; Brown, C. Structural Load Bearing Supercapacitors Using a PEGDGE Based Solid Polymer Electrolyte Matrix. *Proceedings of the ASME 2011 Conference on Smart Materials, Adaptive Structures and Intelligent Systems*, Scottsdale, AZ, 2011.

12. Snyder, J.; Gienger, E.; Wetzel, E.; Xu, K. Energy Density and Rate Limitations in Structural Composite Supercapacitors. *Proc of SPIE Defense Sensing Conference*, Baltimore, MD, 2012.

13. Ajayan, P.; Tour, J. Nanotube Composites. *Nature* **2007**, *447*, 1066–1068.

14. Koetz, R.; Carlen, M. Principles and Applications of Electrochemical Capacitors. *Electrochimica Acta* **2000**, *45*, 2483–2498.

15. Burke, A. *Journal of Power Sources* **2000**, *91*, 37–50.

16. Hahm, M. Diameter Selective Growth of Vertically Aligned Single Walled Carbon Nanotubes and Study on Their Growth Mechanism. *The Journal of Physical Chemistry C* **2008**, *112*, 17143–17147.

17. Mauritz, K.; Moore, R. State of Understanding of Nafion. *Chem Rev* **2004**, *104*, 4535–4585.

18. Lufrano, F.; Staiti, P. Performance Improvement of Nafion Based Solid State Electrochemical Capacitor. *Electrochimica Acta* **2004**, *49*, 2683–2689.

19. Birkmeyer, P.; Peterson, K.; Fearing, R. DASH: a Dynamic 16g Hexapedal Robot. in *Proceedings of the 2009 IEEE/RSJ International Conference on Intelligent Robots and Systems*, St. Louis, MO, 2009.

20. Hoover, A. Bio-inspired Design and Dynamic Maneuverability of a Minimally Actuated Six-legged Robot. in *Proceedings of the 2008 IEE/RAS-EMBS International Conference on Biomedical Robotics and Biomechatronics*, Tokyo, Japan, 2010.

21. Hoover, A.; Fearing, R. Fast Scale Prototyping for Folded Millirobots. *Proceedings of the 2008 IEEE International Conference on Robotics and Automation*, Pasadena, CA, (2008).

22. MatWeb, LLC, MatWeb: Material Property Data, [Online]. Available: www.matweb.com. [Accessed 09 03 2012].

23. Haslach, H. *Deformable Bodies and Their Material Behavior*; Hoboken, NJ: John Wiley & Sons, Inc., 2004.

24. Whatman, Whatman, [Online]. Available: http://www.whatman.com/QualitativeFilterPaperStandardGrades.aspx. [Accessed May 2011].

25. Bradford, P. A Novel Approach to Fabricate High Volume Fraction Nanocomposites with Long Aligned Carbon Nanotubes. *Composites Science and Technology* **2010**, *70*, 1980–1985.

26. Ogasawara, T. Mechanical Properties of Aligned Multi-walled Carbon Nanotube/Epoxy Composites Processed Using a Hot-melt Prepreg Method. *Composites Science and Technology* **2011**, *71*, 1826–1833.

27. Satterfield, M. Mechanical and Water Sorption Properties of Nafion and Composite/Titanium Dioxide Membranes for Polymer Electrolyte Membrane Fuel Cells, *Ph.D. Dissertation*, Princeton Univ (2007).

6. Transitions

We are currently looking into a variety of opportunities to transition this research. The development of multifunctional lightweight, structural-energy storage nanocomposites could benefit a variety of defense related organizations, including the U.S. Army Research, Development and Engineering Centers.

Unfinished/future work for this project includes (1) further test environmental effects on structure performance, (2) synthesize electrospun polymer composite fibers to better control the electrical and mechanical properties of these lightweight structural energy storage materials, and (3) explore other multifunctional structural energy storage materials besides the supercapacitor based designs (traditional capacitors, batteries, etc.). A portion of the year 2 Director's Research Initiative (DRI) funds were used to purchase equipment for the custom electrospinning apparatus shown in figure 15, the assembly of which is currently underway. This setup will allow for the processing of aligned and non-aligned polymer fiber mats.

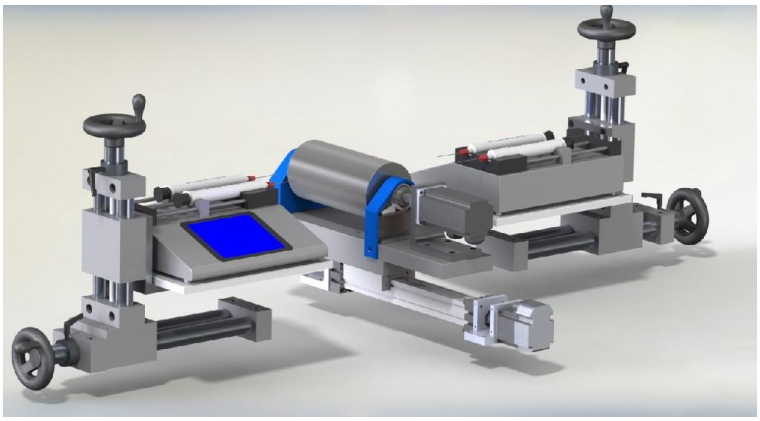

Figure 15. Schematic of electrospinning setup that will allow for the fabrication of polymer and polymer composite fiber mats.

List of Symbols, Abbreviations, and Acronyms

CD	cross-machine direction
CNTs	carbon nanotubes
CV	cyclic voltammetry
CVD	assisted chemical vapor deposition
DASH	Dynamic Autonomous Sprawled Hexapod
DI-H_2O	de-ionized water
DMC	dimethyl carbonate
DMF	dimethylformamide
DRI	Director's Research Initiative
EC	ethylene carbonate
KOH	potassium hydroxide
$LiPF_6$	lithium hexafluorophosphate
MAV	micro aerial vehicle
MD	machine direction
MV	micro-vehicle
MWNTs	multi-walled nanotubes
PDMS	polydimethylsiloxane
PET	polyethylene terephthalate
PVDF	polyvinylidene fluoride
ROEs	randomly oriented electrodes
SDBS	sodium dodecylbenzenesulfonic acid
SEM	scanning electron microscopy
Si	silicon
SPE	solid polymer electrolyte

SWNTs	single wall carbon nanotubes
TEM	transmission electron microscopy
VAEs	vertically aligned electrodes

No of. Copies	Organization
1	ADMNSTR
ELEC	DEFNS TECHL INFO CTR ATTN DTIC OCA 8725 JOHN J KINGMAN RD STE 0944 FORT BELVOIR VA 22060-6218
2 PDFS	US ARMY RESEARCH LAB
9 HCS	ATTN RDRL VTM D P COLE M RIVERA M BUNDY (2 HCS) DY LE (1 HC) M VALCO (1 HC) J RIDDICK (1 HC) A GHOSHAL (1 HC) A HALL (1 HC) J YOO (1 HC) M MURUGAN (1 HC) BLDG 4603 ABERDEEN PROVING GROUND MD 21005
1 HC	US ARMY RESEARCH LAB ATTN RDRL VTA C KRONINGER BLDG 1120B ABERDEEN PROVING GROUND MD 21005
1 HC	US ARMY RSRCH LAB
7 PDFs	ATTN IMAL HRA MAIL & RECORDS MGMT ATTN RDRL CIO LL TECHL LIB ATTN RDRL SER L M ERVIN M DUBEY B PIEKARSKI ATTN RDRL SED C C LUNDGREN C XU ATTN RDRL SER P AMIRTHARAJ ADELPHI MD 20783-1197
5 PDFs	US ARMY RSRCH LAB ATTN RDRL WMM E E NGO ATTN RDRL WMM A E WETZEL D OBRIEN ATTN RDRL WMM G J SNYDER ATTN RDRL WM S KARNA BLDG 4600 ABERDEEN PROVING GROUND MD 21005
TOTAL:	26 (15 PDFS, 11 HCS)